An electron paramagnetic resonance study of the tetragonally distorted Cr^{2+} ion in $SrCl_2$ and BaF_2

1996 J. Phys.: Condens. Matter 8 7179

(http://iopscience.iop.org/0953-8984/8/38/019)

J. Phys.: Condens. Matter **8** (1996) 7179–7190. Printed in the UK

An electron paramagnetic resonance study of the tetragonally distorted Cr^{2+} ion in $SrCl_2$ and BaF_2

P B Oliete, V M Orera and P J Alonso

Instituto de Ciencia de Materiales de Aragón, Universidad de Zaragoza—Consejo Superior de Investigaciones Científicas, Plaza San Francisco s/n, E-50009 Zaragoza, Spain

Received 10 May 1996, in final form 17 June 1996

Abstract. Chromium-doped $SrCl_2$ and BaF_2 have been studied by both EPR and ENDOR spectroscopy. Cr^{2+} ions enter the fluorite structure in distorted substitution cation sites. In both matrices the distortion observed is tetragonal. X- and Q-band EPR measurements at temperatures between 4 and 300 K allowed us to determine the ion symmetry and the following spin-Hamiltonian parameters: $g_\parallel = 1.974(3)$, $g_\perp = 1.997(3)$, $D - a = -2.114(5)$ cm^{-1}, $|a| = 0.018(3)$ cm^{-1} and $A_\perp(^{53}\mathrm{Cr}) = 35 \pm 2$ MHz for BaF_2; and $g_\parallel = 1.974(3)$, $g_\perp = 1.996(4)$, $D - a = -1.979(2)$ cm^{-1}, $|a| = 0.021(3)$ cm^{-1}, $A_\parallel(^{53}\mathrm{Cr}) = 31.2 \pm 1.5$ MHz and $A_\perp(^{53}\mathrm{Cr}) = 43.5 \pm 1.5$ MHz for $SrCl_2$. For BaF_2, the weak superhyperfine interaction of Cr^{2+} with the surrounding F^- ions has been studied by both EPR and ENDOR techniques for $\boldsymbol{B} \parallel [100]$. No ENDOR signals were detected for $SrCl_2$:Cr. The results are tentatively explained in terms of a Jahn–Teller effect corresponding to $T_{2g} \otimes e_g$ coupling strongly stabilized by lattice stresses, although other possible origins for the distortion cannot be completely ruled out.

1. Introduction

Continuous-wave (cw) and pulsed EPR studies of divalent chromium in CdF_2 [1], SrF_2 [2] and CaF_2 [3] have been recently reported. Alkaline-earth halides have matrices which can be used to study ions in eightfold cubic coordination. In all cases the cw-EPR spectra reflected the orthorhombic symmetry of the Cr^{2+} ion. The observed superhyperfine (shf) structures were explained by considering a shf interaction of the Cr^{2+} 3d electrons with the four nearest-neighbouring fluoride ions in a (110) crystal plane. Furthermore, the electron spin-echo envelope modulation (ESEEM) studies performed on CaF_2 [3] and SrF_2 [4] allowed us to determine the shf interaction parameters and fluoride positions up to the third-neighbour shell in the case of SrF_2.

For all of these matrices the origin of the orthorhombic distortion has been associated with a Jahn–Teller (J–T) effect. In fact, it is believed that a quadratic coupling of the $^5T_{2g}$ electronic ground state for this d^4 ion to the e_g and t_{2g} cubic cluster modes leads to an orthorhombic distortion of the fluoride cube compatible with the EPR results [5].

In the present work we have continued the EPR study of divalent chromium in the alkaline-earth halide series. In contrast to the case of CdF_2, SrF_2 and CaF_2 we have found a pure tetragonal distortion for Cr^{2+} in both matrices studied, $SrCl_2$ and BaF_2. From the EPR results we have obtained the g- and zero-field-splitting (ZFS) tensors as well as some components of the $^{53}Cr^{2+}$ hyperfine (hf) tensor. The resolved hf interaction let us unambiguously assign the anisotropic spectra to chromium.

The question now is whether the distortion is associated with a true J–T effect or whether it has a different origin—for example, a perturbing nearest foreign atom or lattice

0953-8984/96/387179+12$19.50

point defect. It is well known that a linear coupling of the electronic state with the cubic e_g modes following the linear J–T theory [6, 7] produces a tetragonal distorted environment as has been proposed by Vallin and Watkins [8] to explain the pure tetragonal symmetry site for Cr^{2+} ions in II–VI compounds. But, in the case of BaF_2 and $SrCl_2$ matrices, besides the absence of any observable dynamical effect, as is the case for Cr^{2+} in CdF_2, SrF_2 and CaF_2, there are two facts that throw some doubt on the assignment of the observed distortion to a J–T effect. These are the unusual narrowness of the EPR lines and the absence of the severe thermal broadening that makes resonance unobservable at high temperatures in the other reported J–T cases. In fact, we have observed a similar behaviour for an oxygen-perturbed Cr^{2+} defect in CaF_2 [3], although we have tried, in the present work, to avoid any controllable source of oxygen sample contamination.

We have studied the superhyperfine interaction of Cr^{2+} ions with their surrounding fluoride ions in BaF_2 by both cw-EPR and ENDOR techniques. However, experimental difficulties prevented us from establishing a definitive model for this system.

To gain more insight into the nature of the tetragonal distortion we have tried another strategy. It is well known that, in chromium-doped alkaline-earth halides, Cr^+ ions can be produced by ionizing radiations. In fact, we have detected cubic Cr^+ ions in liquid-nitrogen-temperature (LNT) x-irradiated $SrCl_2$:Cr [9]. Since the conversion process is purely electronic at this temperature, the evidence is used to support the J–T model. Unfortunately, in the case of BaF_2, cubic Cr^+ was not produced by this procedure. Preliminary results of this work had been communicated at the Eurodim-94 Conference at Lyon [10].

2. Experimental details

The single crystals used in this study were grown in our laboratory using a standard Bridgman method in an argon atmosphere and carbon crucibles. The CrF_3 content in the starting materials ranged from 0.1 to 1%. $SrCl_2$:Cr samples were colourless while strongly doped BaF_2:Cr samples presented a bluish colour corresponding to a broad absorption spectrum whose first maximum appeared at $\approx 17\,000$ cm^{-1}.

The EPR measurements were performed using a Varian E-112 spectrometer working in the X-band and a Bruker ESP-380 for measurements in the Q-band. Liquid-nitrogen-temperature measurements were taken using an immersion quartz Dewar and measurements at lower temperatures were made using an Oxford CF 100 continuous-flow cryostat. A Varian E-257 continuous-flow cryostat was used for the measurements between LNT and 300 K. The magnetic field values were determined with a NMR gaussmeter and the diphenylpicrylhydrazyl (DPPH) signal ($g = 2.0037 \pm 0.0002$) was used to measure the microwave frequency.

ENDOR measurements in the 0.5–32 MHz range were performed at 10 K in a Varian E-112 spectrometer working in the X-band. The radio-frequency radiation from a PTS 160 frequency synthesizer fed the microwave cavity through a 3100LA RF power amplifier.

3. Experimental results and interpretation

We have measured the EPR spectra of $SrCl_2$:Cr and BaF_2:Cr crystals at 9.3 GHz (X-band) and 34.0 GHz (Q-band) as functions of the angle between the crystallographic axes and the external magnetic field $\boldsymbol{B}$. In contrast to the case for the semiconductors CdF_2, SrF_2 and CaF_2, where the unperturbed Cr^{2+} EPR signals decrease below detection limits at temperatures above 40 K [1–4, 8], measurements could be performed on BaF_2 up to 200 K

and on $SrCl_2$ up to 300 K.

In each case we obtained an anisotropic spectrum corresponding to an ion with an electronic spin of 2 in a pure tetragonal symmetry. The observation of hyperfine structure due to the 9.5% natural abundance of the ^{53}Cr isotope led us to associate the spectra with Cr^{2+} ions. The angular dependence of the positions and intensities of the resonance lines can be explained by the following general spin Hamiltonian (SH):

$$\mathcal{H}_0 = \beta(g_\perp(S_xB_x + S_yB_y) + g_\parallel S_zB_z) + DS_z^2 + \tfrac{1}{6}a(S_x^4 + S_y^4 + S_z^4) + \frac{F}{180}(35S_z^4 - 155S_z^2) \tag{1}$$

with $S = 2$ and the defect x-, y- and z-axes being the fourfold axes of the cube.

In equation (1) the SH parameters have their usual meaning. The dominant fine-structure term for both cases studied is D, which produces a splitting of the fivefold spin-degenerate state into a singlet ($M_s = 0$) and two doublets ($M_s = \pm1$ and $M_s = \pm2$) at distances at zero field of $\approx D$ and $4D$ respectively. The transitions between these levels will be labelled by their high-field M_s-values, although the actual states are combinations of $|M_s\rangle$-values.

Depending on the size of D relative to the microwave energy $h\nu_0$, different transitions can be detected. For the X-band ($|D| \gg h\nu_0$) only the 'forbidden' transitions between the $|\pm1\rangle$ and $|\pm2\rangle$ doublets are observed whereas for the Q-band ($|D| \approx h\nu_0$) we can also detect the 'allowed' $|0\rangle \leftrightarrow |\pm1\rangle$ transition.

The sign of D was obtained in both cases through the temperature dependence at low temperatures (4–15 K) of the relative intensities of the $|+2\rangle \leftrightarrow |-2\rangle$ and $|+1\rangle \leftrightarrow |-1\rangle$ transitions. From the position of the $|0\rangle \leftrightarrow |\pm1\rangle$ transition we can determine the value of $D - a - (2/3)F$ [8]. The F-term in equation (1) was expected to be small, and since the spectra are rather insensitive to this parameter we have assumed F to be zero throughout the analyses. The $|a|$-value was obtained from the $|+2\rangle \leftrightarrow |-2\rangle$ to $|+1\rangle \leftrightarrow |-1\rangle$ line intensity ratio, approximately proportional to a^2, in the [110] direction at 77 K.

3.1. $SrCl_2$:Cr^{2+}

X-band EPR measurements were performed on $SrCl_2$:Cr crystals from 4 to 300 K in the crystallographic (110) and (001) planes and in the Q-band at 85 K for the magnetic field rotating in the (001) plane. The line-width increases with the temperature (0.6 mT at LNT and 7.8 mT at RT for the high-field line in the X-band), and above 300 K the lines are so broad that they cannot be measured.

Figure 1 shows the angular dependence for the (001) plane of the Q-band spectrum measured at 85 K. This dependence clearly corresponds to a spin system with tetragonal symmetry. The resonances detected in this plane, labelled in the figure by their defect z-axes (the axes of the tetragonal distortion), correspond to the $|+1\rangle \leftrightarrow |-1\rangle$ transition. The EPR line observed at $\approx$0.9 T for $\boldsymbol{B} \parallel$ [100] direction corresponds to the $|0\rangle \leftrightarrow |+1\rangle$ transition for the $\boldsymbol{z} \parallel$ [100] defect. Measurements at X-band frequencies when the magnetic field is contained in the (110) plane allowed us to observe a new resonance at about 0.12 T for directions around the [$\bar{1}$10] direction. These lines are assigned to the $|+2\rangle \leftrightarrow |-2\rangle$ transition for defects with z-axis$\parallel$ [100] and [010]. At 77 K the intensity of these resonances is much lower than for the $|+1\rangle \leftrightarrow |-1\rangle$ lines. However, for temperatures below 5 K the $|+2\rangle \leftrightarrow |-2\rangle$ transition becomes more intense than the corresponding $|+1\rangle \leftrightarrow |-1\rangle$ transition, showing that $D < 0$.

The experimental resonance positions of the rotational diagram (crosses in figure 1) have been explained using the SH of equation (1). The dashed lines show the transition

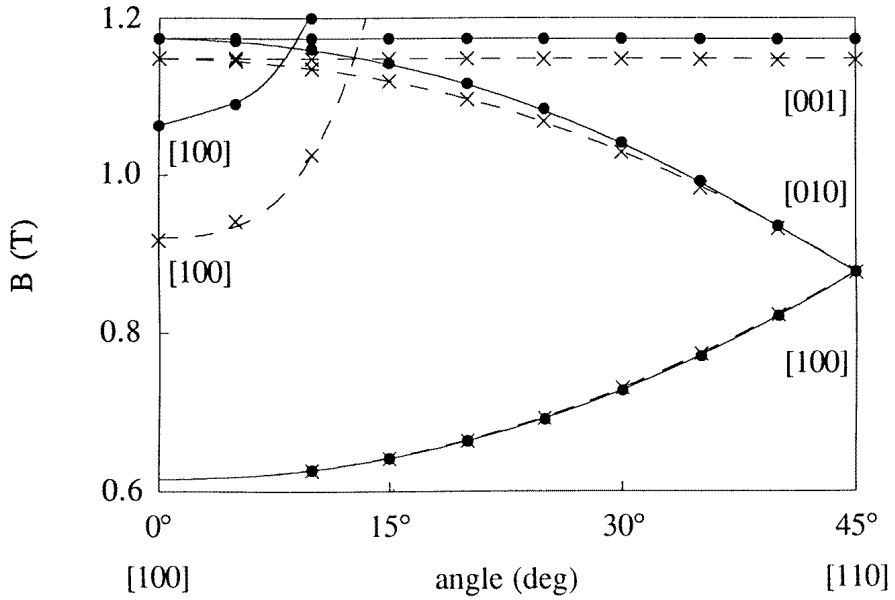

Figure 1. The angular dependence of the EPR line positions for the magnetic field rotating in a (001) plane measured at 85 K in the Q-band. ●: BaF_2; ×: $SrCl_2$. Solid and dashed curves give the calculated line positions obtained using equation (1) and the parameters given in table 1.

Table 1. SH parameters. D, E and a are given in cm^{-1}, and the hf parameters in MHz.

	$SrCl_2$	BaF_2	BaF_2	CaF_2(I)	CaF_2(II)	SrF_2
g_x	1.996(4)	1.997(3)	1.99(1)	1.995(3)	1.99	1.96(1)
g_y	1.996(4)	1.997(3)	1.99(1)	1.995(3)	1.99	1.98(1)
g_z	1.974(2)	1.974(3)	1.942(5)	1.965(7)	1.95	1.94(1)
D	−1.979(2)†	−2.114(5)†	−2.111(3)†	−2.237(5)	−2.8	−2.791(3)
$E - a/6$	—	—	—	0.0476(1)	0.057	0.0283(2)
$\|a\|$	0.021(3)	0.018(3)	—	—	0.073	0.037
$A_\parallel(^{53}Cr)$	31.2 ± 1.5	—	≈ 45	36 ± 4	—	—
$A_\perp(^{53}Cr)$	43.5 ± 1.5	35 ± 2	≈ 45	33.3 ± 3	—	—
z-axis	[100]	[100]	[100]	[110]	[110]	[110]
Reference	This work	This work	Reference [11]	Reference [3]	Reference [3]	Reference [2]

† For the tetragonal cases the D-values given in table 1 correspond actually to the values of $D - a$.

magnetic field values calculated via an exact diagonalization of this SH and the parameters given in table 1. The agreement with the experimental work is excellent. The parameter values are independent of the temperature throughout the measured range.

In agreement with line intensity calculations using the eigenstate set which diagonalize equation (1), the $|+1\rangle \leftrightarrow |-1\rangle$ transition intensity decreases from high field (perpendicular centre) to low field, vanishing when the magnetic field is parallel to the defect z-axis. The rotational diagrams in the (001) and (110) planes for the X-band and the line intensities are also in perfect agreement with the proposed defect symmetry and SH parameters given above.

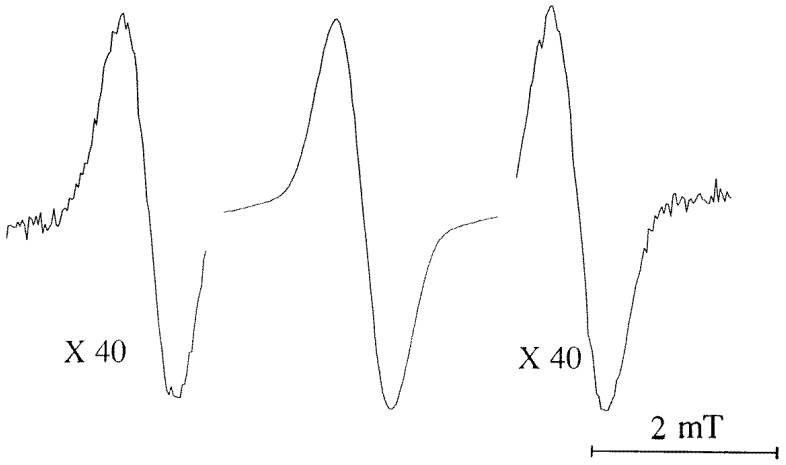

Figure 2. The X-band spectrum of $SrCl_2$:Cr^{2+} corresponding to the $|+1\rangle \leftrightarrow |-1\rangle$ transition measured at 77 K with the magnetic field along a [100] direction perpendicular to the defect z-axis. The spectra on either side of the central line are amplified by 40 for presentation purposes.

3.1.1. hf structure. Figure 2 shows the spectrum corresponding to the high-field $|+1\rangle \leftrightarrow |-1\rangle$ transition for 9.3 GHz in the [100] direction at 77 K. It consists of a central line with two replicas about 40 times weaker on either side. These structures are explained by the hyperfine interaction with the 9.5% naturally abundant ^{53}Cr isotope ($I = 3/2$). From four expected replicas only the two outer lines are observed, the two inner ones falling below the intense central spectrum. The measured splitting between lines is 49.34 MHz. The same structure is observed in the Q-band but with a different splitting (67.21 MHz). This hf splitting is isotropic for the perpendicular defect in the (001) plane.

In order to explain the hf spectrum the following axial SH has been added to that given in equation (1):

$$\mathcal{H}_{hf} = A_{\parallel}(^{53}\mathrm{Cr})S_z I_z + A_{\perp}(^{53}\mathrm{Cr})(S_x I_x + S_y I_y). \tag{2}$$

The parallel axis of the hf axial tensor is chosen to be the defect z-axis (see below). The hyperfine parameters are obtained by applying perturbation methods up to first order as follows.

For $\boldsymbol{B} \parallel [100]$ and perpendicular to the defect z-axis, the expected values of the spin operators are $\langle S_y\rangle = \langle S_z\rangle = 0$ for the two electronic eigenstates involved in the transition, which we will name 1 and 2, and the effective hf splitting (the measured splitting) is

$$A_{eff} = |\langle S_x\rangle_1 - \langle S_x\rangle_2|A_{\perp}. \tag{3}$$

Thus, A_{eff} depends on the microwave frequency as do the electronic eigenstates. Using the eigenstates of the SH given in equation (1) we have calculated $\langle S_x\rangle_1$ and $\langle S_x\rangle_2$ for both X- and Q-band frequencies and thus obtained $A_{\perp} = 43.5$ MHz.

For $\boldsymbol{B} \parallel [110]$ and the $\boldsymbol{z} \parallel [001]$ defect, only the mean value $\langle S_z\rangle$ remains zero. The effective splitting observed in the spectrum is now given by

$$A_{eff} = A_{\perp}\left[\sqrt{\langle S_x\rangle_1^2 + \langle S_y\rangle_1^2} + \sqrt{\langle S_x\rangle_2^2 + \langle S_y\rangle_2^2}\right]. \tag{4}$$

We have calculated $\langle S_x\rangle_j$ and $\langle S_y\rangle_j$. Using equation (4) and the experimental splitting we obtain the same perpendicular hf parameter for this configuration. This implies that the

choice of hf axes is correct. In order to obtain the parallel hf parameter we have analysed the hf spectrum associated with the $|0\rangle \leftrightarrow |+1\rangle$ transition, when the magnetic field is applied parallel to the defect z-axis. As for this case $\langle S_x\rangle = \langle S_y\rangle = 0$ and $\langle S_z\rangle = 0$ or $+1$ depending on the electronic level considered, we can directly obtain

$$A_{\parallel} = A_{eff} = 31.2 \text{ MHz}.$$

The shf interaction with the chloride ions could not be resolved in the EPR spectra, since its structure is included in the resonance line-width. ENDOR signals were not observed for these samples.

3.2. BaF_2:Cr^{2+}

The EPR of BaF_2:Cr was measured at the X- and Q-band frequencies at temperatures between 4 and 200 K. The Q-band EPR angular evolution in the (001) plane at 85 K is shown in figure 1. The anisotropic spectrum corresponds to the $|+1\rangle \leftrightarrow |-1\rangle$ transitions of a Cr^{2+} ion in a tetragonal environment. The $|0\rangle \leftrightarrow |+1\rangle$ transition is also observed for the parallel defect at about 1.06 T when the magnetic field is along the [100] direction. The angular evolution of the resonance positions and the line intensities can be explained using the SH of equation (1), with the best-fitting parameter set given in table 1. The line positions calculated with these parameters and an exact diagonalization of the SH are compared in figure 1 with those which were observed, and the agreement is excellent. The angular dependences of the X-band spectrum when the magnetic field rotates in the (001) and (110) crystal planes also fit within these parameters. The SH parameters are temperature independent. For measurements in the X-band and the magnetic field contained in the (110) plane, a resonance assigned to the $|+2\rangle \leftrightarrow |-2\rangle$ transition is observed at about 0.12 T in the $[\bar{1}10]$ direction. The intensity of these lines, associated with the defects with the z-axis $\parallel$ [100] and z-axis $\parallel$ [010], is much lower than that of the corresponding $|+1\rangle \leftrightarrow |-1\rangle$ signals at 77 K. The different temperature evolutions for the two resonances in the range 4–15 K allow us to determine that $D < 0$.

3.2.1. hf structure. The ^{53}Cr hf interaction is resolved for the perpendicular defect as shown in figure 3. On either side of the central structure, some replicas are seen whose intensity is approximately 40 times lower than that of the central one. As in the case of $SrCl_2$ this splitting is isotropic for the defect perpendicular to the magnetic field. Following the previous procedure we obtained $A_{\perp} = 35$ MHz. Out of this orientation the lines broaden and the hf structure cannot be resolved. As the magnetic field approaches the parallel situation the lines narrow again but their intensities are so low that the hf spectrum is not observed. In this case the $|0\rangle \leftrightarrow |+1\rangle$ line presents a shf structure that prevents us from resolving the parallel hf spectrum, which is at variance with the case for $SrCl_2$.

3.2.2. shf structure. Besides the hf structure, the perpendicular signal consists of five equally spaced lines whose intensities are about 4 and 45 times lower than the central one (see figure 3). The splitting between these lines is isotropic for the perpendicular defect in the (100) plane and close to the fluorine nuclear Zeeman value (21.3 MHz for the X-band). In the X-band, this structure is soon lost as we move away from the perpendicular direction. In contrast, a similar structure is observed in the Q-band in the parallel $|0\rangle \leftrightarrow |+1\rangle$ and perpendicular $|+1\rangle \leftrightarrow |-1\rangle$ transitions, but with only three lines and different relative intensities. In this case the splitting is also close to the fluorine nuclear Zeeman value (42.8 MHz for the parallel field and 47 MHz for the perpendicular field for the Q-band).

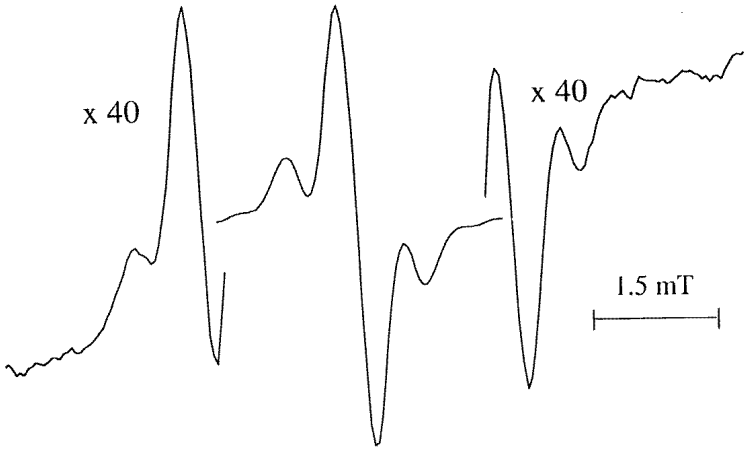

Figure 3. The X-band spectrum of BaF_2:Cr^{2+} corresponding to the high-field $|+1\rangle \leftrightarrow |-1\rangle$ transition measured at 77 K with the magnetic field along a [100] direction. The spectra on either side of the central resonance are amplified by 40 for presentation purposes.

Away from the perpendicular and parallel directions the bands broaden and the structure is not resolved.

ENDOR measurements were made in the X-band at 10 K. Figure 4 shows the ENDOR spectrum obtained when the magnetic field is applied along the [100] direction and perpendicular to the z-axis of the defect. The signal-to-noise ratio is very low and, apart from an intense peak corresponding to the fluorine Larmor frequency (21.3 MHz at the actual magnetic field), only two well defined peaks at 18.8 and 22.3 MHz are observed. For small deviations from this orientation the lines split into several components. Up to four lines can be distinguished from the high-frequency line. Unfortunately, away from the [100] neighbourhood the peaks become confused with the background noise which prevents us from following their angular dependence.

Although the structure is certainly due to interaction with the surrounding fluoride nuclei, there is insufficient experimental information to determine the position of the fluoride ions. The EPR structure and ENDOR spectrum can be explained by the combined effect of superhyperfine and nuclear Zeeman interactions as follows. The absence of any line splitting on rotation in the perpendicular plane, in addition to the number of lines and their intensity ratios, indicate that the transitions are 'nuclear' ones with effective shf constants smaller than the nuclear Zeeman contribution but with an anisotropy large enough to make these transitions partially allowed. Assuming that the nearest-neighbour shell of chromium consists of a tetragonally distorted cube of equidistant fluoride ions, the shf structure seen in the EPR and the ENDOR lines can be explained by adding the following Hamiltonian to equation (1):

$$\mathcal{H}_{shf+nz} = \sum_i (-g_n \beta_n \boldsymbol{I}^i \cdot \boldsymbol{B} + \boldsymbol{S}\mathbf{A}^i \boldsymbol{I}^i) \tag{5}$$

where i ranges from 1 to 8 and the shf tensors $\mathbf{A}^i$ are assumed to be axial along the Cr^{2+}–F^- bonding directions. g_n and β_n are the fluorine nuclear Landé factor and nuclear Bohr magneton respectively.

When the magnetic field is parallel to the defect x-axis (perpendicular defect) the eight

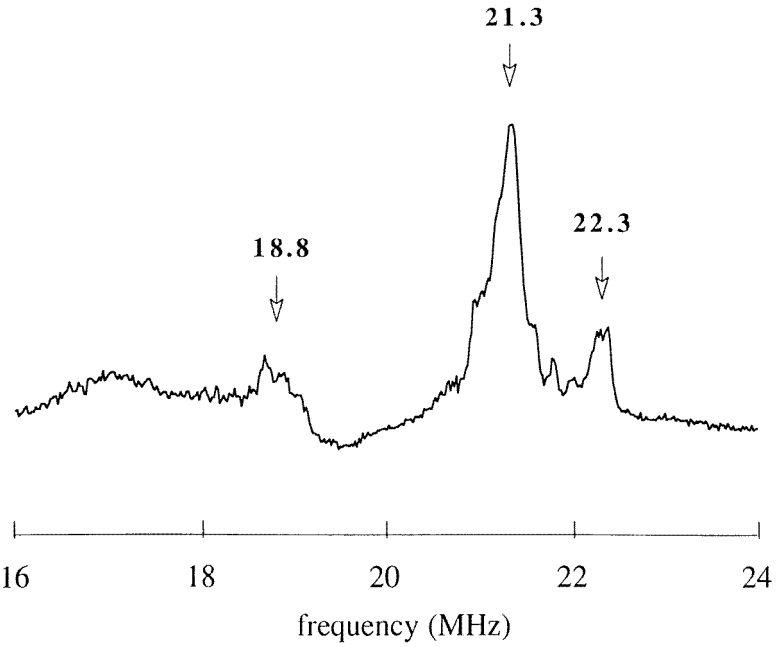

Figure 4. The X-band ENDOR spectrum of BaF_2:Cr^{2+} measured in the [100] direction for $\boldsymbol{B}$ perpendicular to the defect z-axis at 10 K. The intense line at 21.3 MHz corresponds to the fluorine Larmor frequency at the EPR resonance field.

fluoride ions are equivalent and $\langle S_y\rangle = \langle S_z\rangle = 0$. Using perturbation calculations up to first order, the Hamiltonian of equation (5) is reduced to

$$(\mathcal{H}_{shf+nz})_j = \sum_i \{-g_n\beta_n I_x^i|\boldsymbol{B}| + (A_{xx}I_x^i + A_{yx}I_y^i + A_{zx}I_z^i)\langle S_x\rangle_j\} \tag{6}$$

with x, y, and z being the defect axes and $j = 1$, 2 standing for the electronic state considered. From the eigenvalues of equation (6), c_j, the splittings between the nuclear states are easily calculated to be

$$\Delta_j = 2c_j = \sqrt{\langle S_x\rangle_j^2(A_{xx}^2 + A_{yx}^2 + A_{zx}^2) + (g_n\beta_n|\boldsymbol{B}|)^2 - 2\langle S_x\rangle_j A_{xx} g_n\beta_n|\boldsymbol{B}|}. \tag{7}$$

We realize that if

$$\langle S_x\rangle_j^2(A_{xx}^2 + A_{yx}^2 + A_{zx}^2) - 2\langle S_x\rangle_j A_{xx} g_n\beta_n|\boldsymbol{B}| \approx 0$$

the transitions would be equally spaced with a splitting near to the nuclear Zeeman one, as observed. In addition, the effective shf splitting depends on the electronic state and it can be smaller than the shf constant. In particular for the X-band $\langle S_x\rangle \approx 0.15$ and $\langle S_x\rangle \approx 0.9$ for the $|\pm 1\rangle$ levels considered here. This explains the observation of two ENDOR peaks non-symmetrically placed with respect to the fluorine Larmor line (21.3 MHz) when $\boldsymbol{B} \parallel [100]$.

The mixing coefficients for the nuclear eigenstates in the $|\pm 1/2\rangle_x$ basis are

$$u_j = \frac{b_j}{\sqrt{|b_j|^2 + (c_j - a_j)^2}} \qquad \text{and} \qquad v_j = \frac{(c_j - a_j)}{\sqrt{|b_j|^2 + (c_j - a_j)^2}} \tag{8}$$

with

$$a_j = \frac{\langle S_x\rangle_j}{2}A_{xx} - \frac{g_n\beta_n|\boldsymbol{B}|}{2} \tag{9}$$

and

$$b_j = \frac{\langle S_x \rangle_j}{2}(A_{zx} + \mathrm{i}A_{yx}). \tag{10}$$

In order to have a non-zero intensity for the 'forbidden transitions' it is necessary that $b_j \neq 0$ and $u_1 \neq u_2$, $v_1 \neq v_2$. The first condition requires an anisotropic superhyperfine interaction, whereas $\langle S_x \rangle_1 \neq \langle S_x \rangle_2$ satisfies the second condition. The $\langle S_x \rangle_j$ are different for the Q- and X-bands, and therefore the nuclear eigenstate mixing is also different. Thus, the relative intensities of allowed and forbidden transitions depend on the microwave frequency, as is observed experimentally.

Next we can use the ENDOR results to gain some insight into the shf constant values. In order to estimate the value of the shf interaction parameters we propose a Cr^{2+} environment consisting of eight fluoride ions out of their undistorted lattice sites but in the (110) crystal planes. We have two data values and three unknowns (A_{xx}, A_{yx}, A_{zx}) that can be written as a function of the isotropic and anisotropic shf constants a and b and the angle θ between the [110] cubic axis and the Cr^{2+}–F^- bonding directions, with

$$A_{xx} = a + \frac{b}{2}(1 - 3\sin^2\theta)$$
$$A_{yx} = \frac{3}{2}b\cos^2\theta$$
$$A_{zx} = \frac{b}{\sqrt{2}}3\cos\theta\sin\theta.$$

Taking a reasonable value for θ, $25^\circ < \theta < 50^\circ$, we obtain $a = -6 \pm 4$ MHz and $|b| = 8 \pm 1$ MHz. As can be seen, $|b|$ is rather insensitive to the bonding angle whereas the a-value has a large uncertainty. The intensity ratio between the forbidden and allowed nuclear transitions increases with the anisotropy, and is close to the experimental value for $|b| \approx 8.5$ MHz and $\theta = 45^\circ$. Also, the predicted shf splittings are low enough to remain within the halfwidth of the EPR lines over all of the measured range. Thus a model consisting of a tetragonally elongated fluoride cube is in agreement with the experimental data obtained.

After we completed this work, a publication on Cr^{2+} in BaF_2 appeared [11]. The symmetry of the defect and the similarity of some of the SH parameters given by the authors led us to realize that it is the same centre as we have studied. Using a simplified crystal-field analysis, these authors propose a defect model consisting of an off-centre Cr^{2+} ion for BaF_2. In our opinion this model is not sufficiently supported by their experimental results. In fact, there is a discrepancy in $g_{||}$ (1.942 versus 1.974) and in the $^{53}Cr^{2+}$ hyperfine parameters ($A_{||} \approx A_\perp \approx 45$ MHz versus 35 MHz) that could be due to some possible experimental difficulties in the EPR rotational diagrams. $g_{||}$ is mainly determined from the low-field signal appearing close to the [100] direction (for $\boldsymbol{B} \parallel$ [100] its intensity is zero). By measuring the angular dependence of the EPR lines in the (001) plane we were able to detect the 'parallel' signal down to 10° from the [100] direction thus giving a good value for $g_{||}$. In reference [11] it seems that by measuring in the (011) plane they could only detect this signal above 25° off the [100] direction, and therefore their determination of $g_{||}$ is less accurate. This is very important if crystal-field theory is used to determine the defect model, as is done in reference [11]. Besides the strong approximations needed when using this theory, the results are very sensitive to the g-shifts, and small deviations can give large changes in the energy level diagram.

4. Discussion

As we have established in the preceding section, Cr^{2+} ions are in non-cubic environments in BaF_2 and $SrCl_2$. The first point that we want to discuss is the origin of these distortions.

The EPR line-shapes are gaussian-like and the spectra do not show any behaviour typical of weak or moderate J–T coupling as described, for example, by Bill [12]. We therefore have to consider a static J–T distortion where the effect of some random stresses of the appropriate symmetry stabilizes the system in one of the possible J–T distortions, leading to the 'conventional' low-symmetry EPR spectra observed. This is usually the case for 3d ions in fluorites [13].

From our EPR experiments it is difficult to distinguish between a static J–T effect and a low-symmetry crystal-field perturbation due, for example, to an unwanted impurity or lattice defect or an off-centre system. Since the solubility of Cr^{2+} in those crystals is rather low, it could, in principle, be related to any unidentified impurity or intrinsic defect. In favour of an unperturbed Cr^{2+} ion is the fact, already mentioned in the introduction, that cubic Cr^{+} ions can be produced by 77 K x-irradiation in $SrCl_2$ [9]. At this temperature the intrinsic defects and the impurities are not mobile and we can safely assume that the valence change is a consequence of a pure electronic process. It is interesting to note that trigonal Cr^{+} is obtained in $SrCl_2$ when the irradiation is performed at RT, at which both chloride vacancies and interstitial anions are mobile.

We have x-irradiated $SrCl_2$ samples at LNT. We observed that the Cr^{+}-ion concentration increases when the Cr^{2+}-ion concentration decreases. This experiment can be used to associate the Cr^{2+} ion with an intrinsic defect, not stabilized by a foreign atom. However, the possibility of an off-centre Cr^{2+} ion still cannot be ruled out.

Off-centre ions in ionic systems usually occur when either the ion is small or it has a large polarizability [14]. From these steric considerations there is no reason for having off-centre Cr^{2+} and cubic Cr^{+} in the same matrix, not least since the latter is smaller than the former.

In crystals with the fluorite structure, off-centre displacements along the fourfold axis have been observed in d^9 ions such as Ag^{2+}, Cu^{2+} and Ni^{+} [15–17]. Although the reason for this behaviour is not yet fully understood, it is clear that it is not related to the ion size but is probably due to the configuration interaction with p orbitals favouring the coupling to t_{1u} modes (the pseudo-J–T effect) [12]. Against a similar situation for d^4 ions we can argue that it does not occur in CaF_2, and CdF_2, and that in other matrices Cr^{2+} coupling to e_g modes is usually strong enough to produce static J–T effects.

In fact, the pure tetragonal distortion observed is indeed compatible with the J–T effect. If a strong linear coupling of the electronic ground state T_{2g} to the cubic cluster e_g mode is considered, three minima in the Q-space corresponding to the tetragonal distortion are obtained [7]. Stabilization of the J–T distortion by lattice strains of E symmetry would explain the observation of static spectra as well as the narrowness of the resonance lines.

The situation is not so clear for BaF_2:Cr. We have not found evidence of cubic Cr^{+} production by LNT x-irradiation in this system. The study of the shf structure, both by EPR and ENDOR techniques, has only provided some incomplete information about the fluoride coordination shell. We can safely state that Cr^{2+} interacts with at least four fluoride ions, presumably equivalent for $\boldsymbol{B} \parallel [100]$, but we cannot determine their positions.

Although we have avoided sample contamination during the crystal growth process, we cannot, in principle, rule out the possible presence of small amounts of unwanted impurities, which may produce the stabilization of the tetragonal distortion for Cr^{2+} in BaF_2. However, the fact that our results are compatible with a pure tetragonal distortion of the fluoride cube

leads us to propose, with some reservations, a J–T effect for this ion.

Thus—and adding the results of previous studies on CdF_2 [1], SrF_2 [2] and CaF_2 [3] to the present ones—we can almost establish a complete picture for divalent chromium in fluorite-type crystals. When the Cr^{2+} ion (ionic radius 0.89 Å) enters the fluorite lattice with a small lattice constant as in CdF_2 (5.46 Å), SrF_2 (5.79 Å) and CaF_2 (5.38 Å), it occupies orthorhombic symmetry sites. However, when the lattice constant increases, as in BaF_2 (6.2 Å) and $SrCl_2$ (6.97 Å), the symmetry of the Cr^{2+}-ion site is tetragonal.

A possible explanation for this situation has been already advanced in a previous paper [3] and deals with the ion displacements corresponding to the ML_8 e_g and t_{2g} vibration modes. In fact, it is expected that electron–phonon coupling to the radial t_{2g} mode causing the orthorhombic distortion will be stronger for the tighter CdF_2, SrF_2 and CaF_2 lattices, whereas coupling to the transverse e_g mode is dominant in the $SrCl_2$ and BaF_2 crystals.

We will now comment on the SH that we have used to interpret the EPR data and on the parameters obtained.

A detailed dynamic J–T model has been developed by Abhvani *et al* [18] for the tetragonal GaAs:Cr^{2+} system. The J–T model involves the derivation of an effective Hamiltonian for the vibronic ground states of the system as well as the calculation of the reduction factors. If appropriate random strains are included, the motion is confined to a potential well: this has been studied in detail for the $T_2 \otimes e$ coupling [18]. In this case the lowest states are orbital singlets with a small degree of mixing caused by the dynamic J–T effect with the states coming from the orbital triplet, and the use of the conventional SH to study the EPR of ground states is fully justified [19].

We will now analyse the values of the SH parameters corresponding to Cr^{2+} ions. In the case of Cr^{2+} in CaF_2, two different defects are obtained [3], depending on the chromium salt used in the growth procedure. For samples grown with Cr_2O_3, Cr^{2+}(I) is obtained, with an orthorhombic distortion associated with an oxygen impurity, whereas for samples grown with CrF_3, the centre detected is Cr^{2+}(II), a purely J–T orthorhombically distorted ion. Firstly it is interesting to note that the parameters given in table 1 are very similar to those of Cr^{2+} in other J–T systems, although they present smaller deviations from the free-electron g-value and a larger homogeneity through the series than in II–VI compounds [8]. We can thus discuss our results using the theoretical models developed for these compounds.

Assuming a point-ion model for the tetragonal cluster, the following expressions for g-factors and the zero-field splitting as a function of the spin–orbit coupling constant λ and the excited-electronic-state energies E_2 (approximately equal to the cubic-field splitting) and $E_1 = 3E_{J-T}$ were proposed:

$$g_{\parallel} = 2.0023 - 8\lambda/E_2 \tag{11}$$

$$g_{\perp} = 2.0023 - 2\lambda/E_1 \tag{12}$$

and

$$D = \lambda^2(1/E_1 - 4/E_2) - 3\rho \tag{13}$$

where ρ stands for the spin–spin interaction [8]. Taking the free-ion values for λ (57 cm^{-1}) and ρ (0.42 cm^{-1}), from $g_{\parallel}$ we obtain $E_2 \approx 16\,200$ cm^{-1} which is very close to the optical absorption band energy of Cr^{2+} in BaF_2. On the other hand it is impossible to fit $g_{\perp}$ and D to equations (12) and (13).

The same problem has also been observed for II–VI compounds. To avoid it, Vallin and Watkins [8] introduced the ligand orbital admixtures to the ground state, thus accounting for the D- and $g_{\parallel}$-values. In any case, $g_{\perp}$-values were not well predicted.

Later on, Abhvani *et al* [18] reviewed that work and concluded that a dynamic model could be necessary to explain the SH parameters. In fact, in a J–T system, there are several excited states below the electronic E_g doublet which can be admixed with the ground state by the spin–orbit interaction. The SH parameters can be then fitted to this dynamical model although the number of parameters is increased.

In our case, ligand contributions are expected to be smaller than in II–VI compounds since the ionicity of fluorites is much larger. So we believe that a dynamical model would also explain the Cr^{2+} SH parameters of alkaline-earth halides.

Acknowledgments

We are grateful to Dr L Lezama from Bilbao University for helping us with some of the Q-band experiments. This research was sponsored by CICYT under contracts MAT-92-1279 and PB92-0040. One of us, PBO, thanks the Diputación General de Aragon for a grant.

References

[1] Jablonski R, Domanska M, Krukowska-Fulde B and Nievnyski T 1973 *Mater. Res. Bull.* **8** 749
[2] Zaripov M M, Tarasov V F, Ulanov V A, Shakurov G S and Popov M L 1995 *Phys. Solid State* **37** 437
[3] Oliete P B, Orera V M and Alonso P J 1996 *Phys. Rev.* B **53** 3047
[4] Oliete P B, Orera V M and Alonso P J 1996 *Phys. Rev.* B at press
[5] Bates C A, Dunn J L and Sigmund E 1987 *J. Phys. C: Solid State Phys.* **20** 1965
[6] Jahn H A and Teller E 1937 *Proc. R. Soc.* A **161** 220
[7] Opik U and Pryce M L H 1957 *Proc. R. Soc.* A **238** 425
[8] Vallin J T and Watkins G D 1974 *Phys. Rev.* B **9** 2051
[9] Orera V M, Alcala R and Alonso P J 1986 *J. Phys. C: Solid State Phys.* **19** 607
[10] Oliete P B, Orera V M and Alonso P J 1995 *Radiat. Eff.* **135** 179
[11] Zaripov M M, Tarasov V F, Ulanov V A and Shakurov G S 1996 *Phys. Solid State* **38** 249
[12] Bill H 1984 *The Dynamical Jahn–Teller Effect in Localized Systems* ed Yu E Perlin and M Wagner (Amsterdam: North-Holland)
[13] Gelhoff W and Ulrici W 1980 *Phys. Status Solidi* b **102** 11
[14] Stoneham A M 1975 *Theory of Defects in Solids* (Oxford: Clarendon)
[15] Bill H, Milleret C and Lacroix R 1973 *Colloque Ampere XVII, Compte Rendue* ed V Hovi (cited in [12], pp 812–4)
[16] Bill H 1973 *Solid State Commun.* **44** 101
[17] Alonso P J, Casas-Gonzalez J, den Hartog H W and Alcala R 1983 *Phys. Rev.* B **27** 2722
[18] Abhvani A S, Austen S P, Bates C A, Parker L W and Pooler D R 1982 *J. Phys. C: Solid State Phys.* **15** 2217
[19] Abhvani A S, Bates C A and Pooler D R 1984 *J. Phys. C: Solid State Phys.* **17** 1713